Scientific Research and Essays Vol. 7(6), pp. 636-646, 16 February, 2012
Available online at http://www.academicjournals.org/SRE
DOI: 10.5897/SRE11.529
ISSN 1992-2248 ©2012 Academic Journals

Full Length Research Paper

Numerical simulation of dynamic pore water pressure using wave theory concept

Abdoullah Namdar

Faculty of Civil Engineering and Earth Resources, University Malaysia, Pahang, Malaysia.
E-mail: anamdar@ump.edu.my, ab_namdar@yahoo.com.

Accepted 4 October, 2011

The seismic force on structure causes instability and could overturn or create unacceptable differential settlement. This paper presents and discusses experimental, theoretical and numerical methods for the study and evaluation of interaction between sandy saturated subsoil and embankment in presence of confined sandy dense column. It is very important predicting structure differential settlement due to dynamic force. For evaluation, dynamic liquefaction ability on sandy model, eight models have been studied. And wave formulas have been employed. The result revealed that the dense zone installed in the subsoil is controlled by the dynamic liquefaction, but it has been observed that after dynamic force mitigated still, some level of dynamic pore water pressure has been appeared and caused differential settlement. This study indicated that the dense zone could only minimize the differential settlement, and it is not able to convert dynamic pore water pressure to linear force, and as long as, dynamic force creates settlement, it is differential settlement. The dynamic pore water pressure act like a wave in vertical direction and if excess higher than limitation creates differential settlement or structure turnover.

Key words: Modeling, dynamic liquefaction, wave formula, differential settlement, seismic mitigation.

INTRODUCTION

A number of researchers have been investigated on liquefaction as a devastative parameter. In an investigation on the experimental studies on sands liquefaction subjected to cyclic loading, It has been observed that the effective stress eventually reach a value close to zero in each cycle (Abdoullah, 2010; Lee and Santamarina, 2007; Verdugo and Ishihara, 1996; Nemat-Nasser and Tobita 1982; Koseki et al., 2000; Vaid and Chern, 1985; Arulmoli et al., 1992; Sivathayalan, 2000), and the majority of seismic damages were caused by permanent ground deformations such as fault movements, landslides and liquefaction (Ariman and Muleski, 1981; Liang and Sun, 2000).

These tests have also been utilized to measure the magnitude of liquefaction in subsoil when dense wall is present and absent. In the present note, an attempt has been made to determine the liquefaction level for different relative dense wall size, density and location for saturated sandy subsoil (Abdoullah, 2010). From the available literature, it is known that due to the complicated site structural geology, it is not an easy task to obtain precisely the exact liquefaction location and force during an earthquake (Liang and Sun, 2000).

Therefore, for studying dynamic liquefaction behavior, several different models for interpretations have been evaluated, namely; (i) the first is not mitigated embankment and (ii) the second is mitigated embankment.

In addition, the wave formulas have been used for analysis of accurate dynamic liquefaction force, and finding an acceptable method for predicting differential settlement on the model.

METHODOLOGY AND EXPERIMENTS

In the present study, shaking table was used for vibrating in one direction and one type of transducers namely; pore pressure sensor was used to measure the excess pore water pressure developed during dynamic loading.

Figure 1 shows that the transducers location was used in the experiment. The sand was used for modeling, and Table 1 shows the dry sand characteristics while Figures 2 to 9 indicated several sandy embankment models (Abdoullah, 2010). In the second part

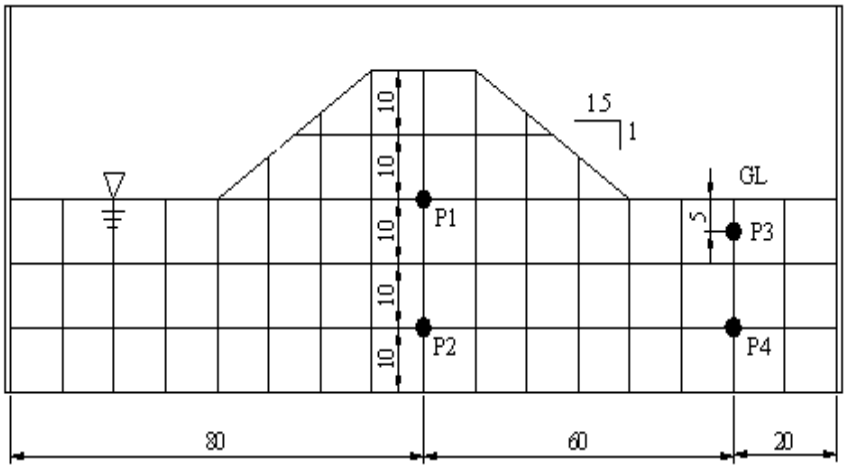

Figure 1. Position of transducers in all modes (Abdoullah, 2010).

Table 1. Physical properties of sand used.

Specific Gravity (G)	2.673
Maximum Void ratio e_{max}	1.15
Minimum Void ratio e_{min}	0.58
Mean Diameters	
D_{10} (mm)	0.39
D_{30} (mm)	0.47
D_{60} (mm)	0.56
Uniformity coefficient Cu	1.22
Coefficient of curvature Cc	1.53
Bulking of sand (%)	4.0

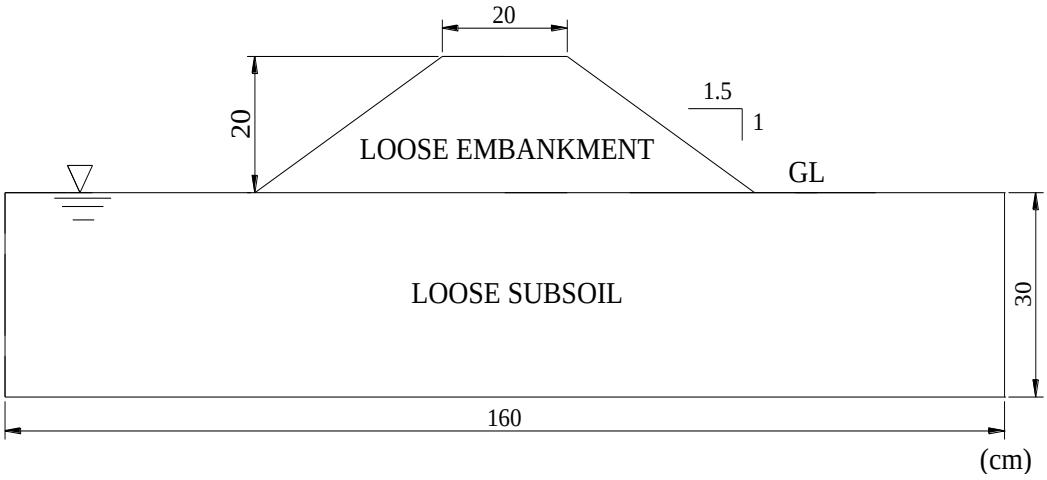

Figure 2. In model 1, the moist loose embankment and fully saturated subsoil (Abdoullah, 2010).

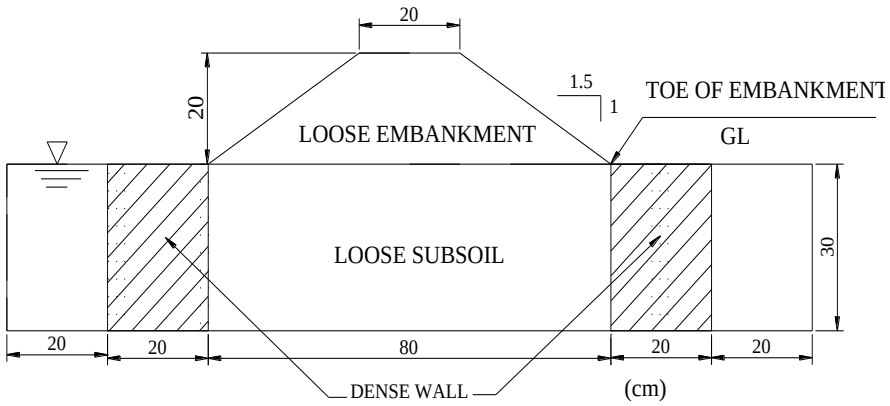

Figure 3. In model 2, the moist loose embankment and fully saturated subsoil. The sandy dense wall of 20 cm thickness installed in the subsoil in exterior toe of embankment (Abdoullah, 2010).

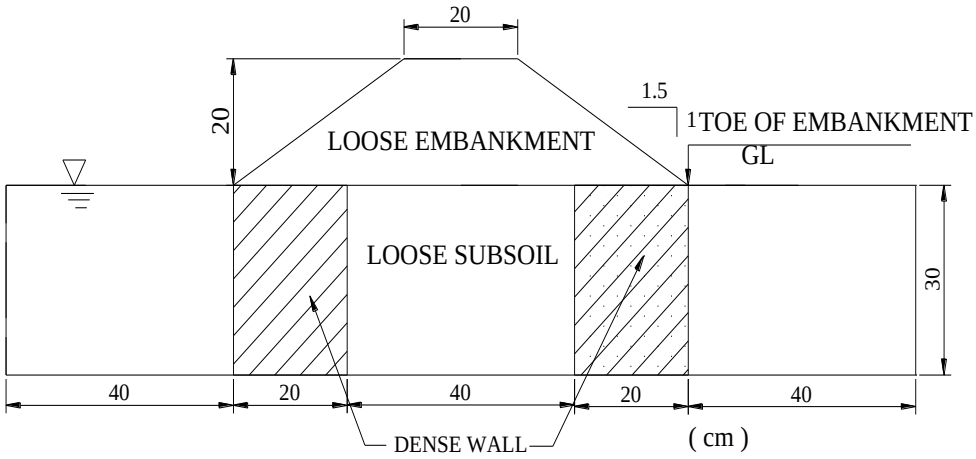

Figure 4. In models 3, the moist loose embankment and fully saturated subsoil. The sandy dense wall of 20 cm thickness installed in the subsoil in interior toe of embankment (Abdoullah, 2010).

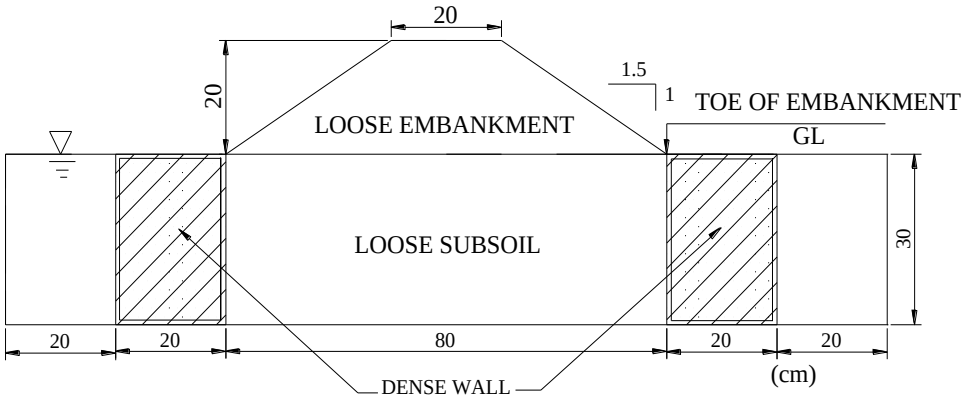

Figure 5. In model 4, the moist loose embankment and fully saturated subsoil. The sandy dense wall of 20 cm thickness, confined in geo textile installed in the subsoil in exterior toe of embankment (Abdoullah, 2010).

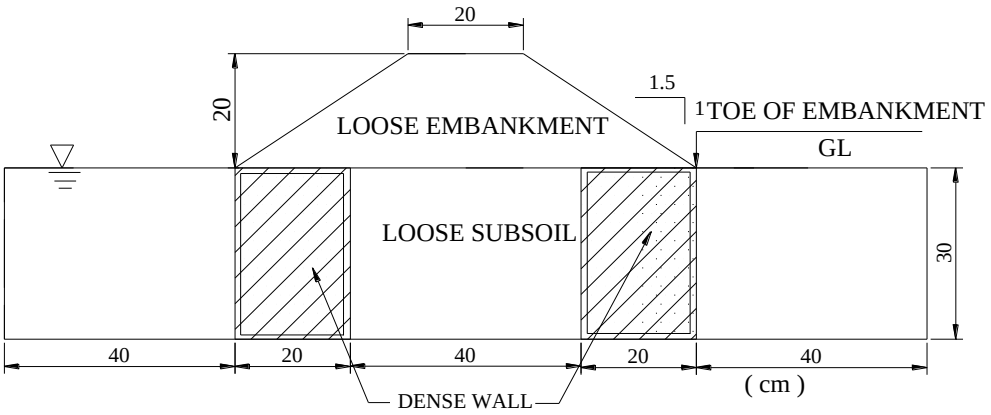

Figure 6. In model 5, the moist loose embankment and fully saturated subsoil. The sandy dense wall of 20 cm thickness, confined in geotextile installed in the subsoil in interior toe of embankment (Abdoullah, 2010).

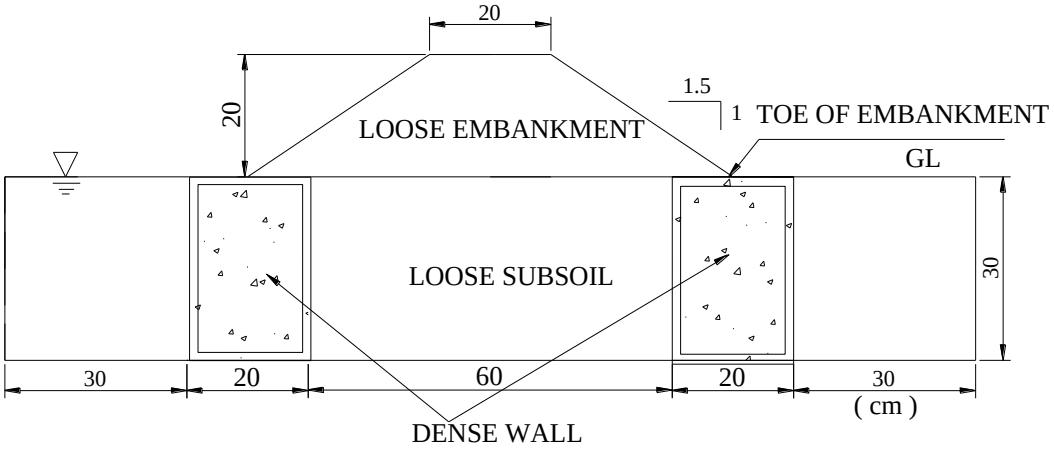

Figure 7. In model 6, the moist loose embankment and fully saturated subsoil. The dense wall made up from composition of 60 % sand and 40 % gravel, 20 cm thickness and confined in geo textile centrally installed beneath the toe of embankment (Abdoullah, 20101).

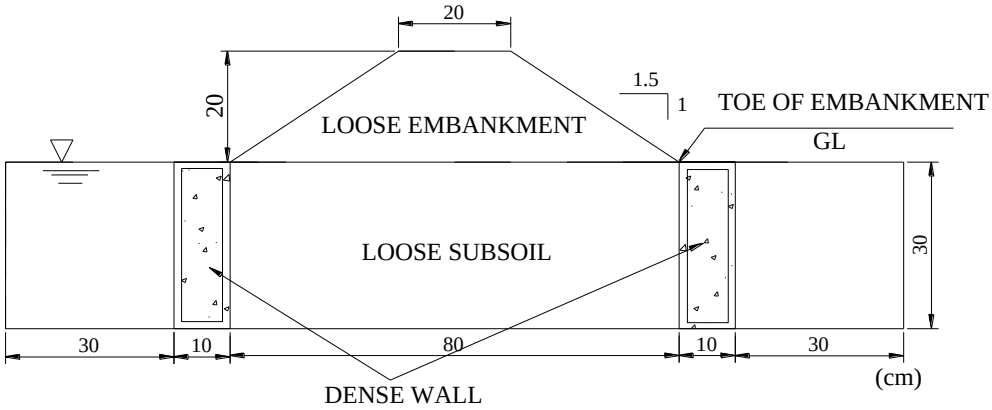

Figure 8. In model 7, the moist loose embankment and fully saturated subsoil. The dense wall made up from composition of 60 % sand and 40 % gravel, 10 cm thickness and confined in geo textile installed in the exterior toe of embankment (Abdoullah, 2010).

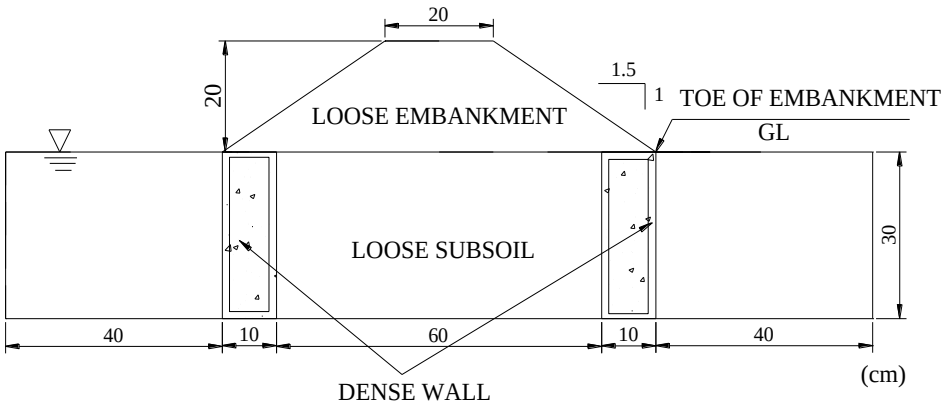

Figure 9. In model 8, the moist loose embankment and fully saturated subsoil. The dense wall made up from composition of 60 % sand and 40 % gravel, 10 cm thickness and confined in geo textile installed in the interior toe of embankment (Abdoullah, 20101).

Table 1. Physical properties of sand used.

Specific Gravity (G)	2.673
Maximum Void ratio e_{max}	1.15
Minimum Void ratio e_{min}	0.58
Mean Diameters	
D_{10} (mm)	0.39
D_{30} (mm)	0.47
D_{60} (mm)	0.56
Uniformity coefficient Cu	1.22
Coefficient of curvature Cc	1.53
Bulking of sand (%)	4.0

of the study, the wave theory concept have been used for numerical simulation of vertical dynamic pore water pressure, which is a wave in the vertical direction, and is one of the major forces on a structure subjected to earthquake.

RESULTS AND DISCUSSION

Interaction between soils and geosynthetics is of utmost importance in applications of these materials as reinforcement in geotechnical engineering. That is also the case for some applications of geosynthetics in environmental protection works. The mechanisms of soil–geosynthetic interaction can be very complex, depending on the type and properties of the geosynthetic and the soil (Ennio, 2009). There are series of finite element analysis which were performed on a prototype slope using two-dimensional plane strain model using the computer code Plaxis. The soil was represented by non-linear hardening soil model, which is an elasto-plastic hyperbolic stress–strain model while reinforcement was represented by elastic elements. Test results indicate that the inclusion of geogrid layers in the replaced sand not only significantly improves the footing performance but also led to great reduction in the depth of reinforced sand layer required to achieve the allowable settlement (Mostafa and Sawwaf, 2007). Along with the dynamic force, the site geological characteristics and some time position of geomembrane could also be a reason for differential settlement or structure overturn. It is well known that the liquefaction on sandy subsoil is an important geotechnical problem. Tables 2 to 3 show numerical simulation of different liquefaction characteristics which are recorded by pore pressure sensors P_2 and P_4. It is assumed that the wave is created from incompressible material and constant in the shape.

Table 2. The characteristics of liquefaction recorded by P4.

c^2	η	ζ_h	ζv	u	w	$\frac{\partial u}{\partial t}$	$\frac{\partial w}{\partial t}$	P	c_G	E	P_E	S_{xx}	S_{yy}
0.014	-0.051	-0.07	-0.05	-1	-0.9	-64.86	-44.9	-60.7	0.0072	0.6452	0.005	0.323	8.89E-29
0.003	-0.017	0.047	-0.02	-0	0.53	58.918	-22	-55.4	0.0014	0.1991	3E-04	0.1	5.47E-59
0.003	-0.024	0.066	-0.02	-0	0.79	68.331	-25.5	-56.5	0.0017	0.3903	6E-04	0.195	1.07E-58
0.003	0.049	-0.01	0.05	0.7	-0.1	-19.41	95.42	-44.8	0.0015	0.1991	3E-04	0.1	6.56E-71
0.005	-0.028	0.075	-0.03	-0	1.09	99.927	-37.3	-57	0.0024	0.5098	0.001	0.255	1.40E-58
0.002	0.0339	-0.01	0.03	0.4	-0.1	-19.64	76.39	-47.2	0.0008	0.0976	8E-05	0.049	4.01E-89
0.001	0.0339	-0.01	0.03	0.4	-0.1	-14.6	56.77	-47.2	0.0006	0.0976	6E-05	0.049	4.01E-89
0.003	-0.014	0.037	-0.01	-0	0.44	63.363	-23.6	-54.8	0.0015	0.1275	2E-04	0.064	3.50E-59

Table 3. The characteristics of liquefaction recorded by P2.

c^2	η	ζ_h	ζv	u	w	$\frac{\partial u}{\partial t}$	$\frac{\partial w}{\partial t}$	P	c_G	E	P_E	S_{xx}	S_{yy}
0.004	0.0291	-0.007	0.03	0.6	-0.2	-54.55	212.2	-47.9	0.0022	0.0717	2E-04	0.036	2.949E-89
0.004	0.0145	-0.004	0.01	0.3	-0.1	-45.09	175.4	-50.3	0.0018	0.0179	3E-05	0.009	7.374E-90
0.004	0.0242	-0.01	0.02	0.5	-0.1	-45.09	175.4	-48.7	0.0018	0.0498	9E-05	0.025	2.048E-89
0.004	0.0145	-0.004	0.01	0.3	-0.1	-45.09	175.4	-50.3	0.0018	0.0179	3E-05	0.009	7.374E-90
0.003	0.0242	-0.006	0.02	0.4	-0.1	-34	132.3	-48.7	0.0014	0.0498	7E-05	0.025	2.048E-89
0.002	0.0145	-0.004	0.01	0.2	-0.1	-24.25	94.31	-50.3	0.001	0.0179	2E-05	0.009	7.374E-90
0.003	0.0145	-0.004	0.01	0.3	-0.1	-40.08	155.9	-50.3	0.0016	0.0179	3E-05	0.009	7.374E-90
0.168	-0.016	0.012	-0.02	-0	0.12	31.882	-42.3	-55.1	0.084	0.0319	0.003	0.016	6.662E-08

For calculation of liquefaction characteristics, the Formula 1 to 18 has been used (Turgut and Michael, 1981). The model without mitigation has been affected more by wave speed, angular frequency, wave number, wave phase angle, velocity potential, dispersion relation, surface elevation, horizontal and vertical particle displacement, horizontal and vertical particle velocity, horizontal and vertical particle acceleration, pressure, group velocity, average energy density, energy flux and radiation stress in x and y direction. The investigation indicated that the wave theory has acceptable ability for explaining these parameters during a dynamic liquefaction.

The Figures 10 to 17, indicated pore water pressure in the model in different location. This investigation indicated that the numerical study is acceptable and is more valid as compared to previous research investigation (Abdoullah, 2010), the wave theory concept could better explain liquefaction characteristics. The dynamic pore water pressure is minimized but there is no possibility for eliminating or converting to the linear force and as long as, dynamic force creates settlement, it is differential settlement. The dynamic pore water pressure act like a wave in vertical direction and if excess higher than limitation creates structure turnover. It is a method for predicting the differential settlement of structure which was too complicate from previous work.

H = Wave height; L = Wave length; T = Wave period = is the time interval between two successive crest

$$C = \text{Wave speed} = \frac{L}{T} \quad (1).$$

$$\omega = \text{Angular frequency} = \frac{2\pi}{T} \quad (2)$$

$$K = \text{Wave number} = \frac{2\pi}{L} \quad (3)$$

$$\theta = \text{Wave phase angle} = kx - \omega t \quad (4)$$

$$\Phi = \text{velocity potential} = \frac{\pi H}{kT}\frac{\cosh(ks)}{\sinh(kd)}\sin\theta \quad (5)$$

$$c^2 = \text{Dispersion relation} = \frac{\omega^2}{k^2} \quad (6)$$

$$\eta = \text{Surface elevation} = \frac{H}{2}\cos\theta \quad (7)$$

$$\zeta_h = \text{Horizontal particle displacement} = \frac{H}{2}\frac{\cosh(ks)}{\sinh(kd)}\sin\theta \quad (8)$$

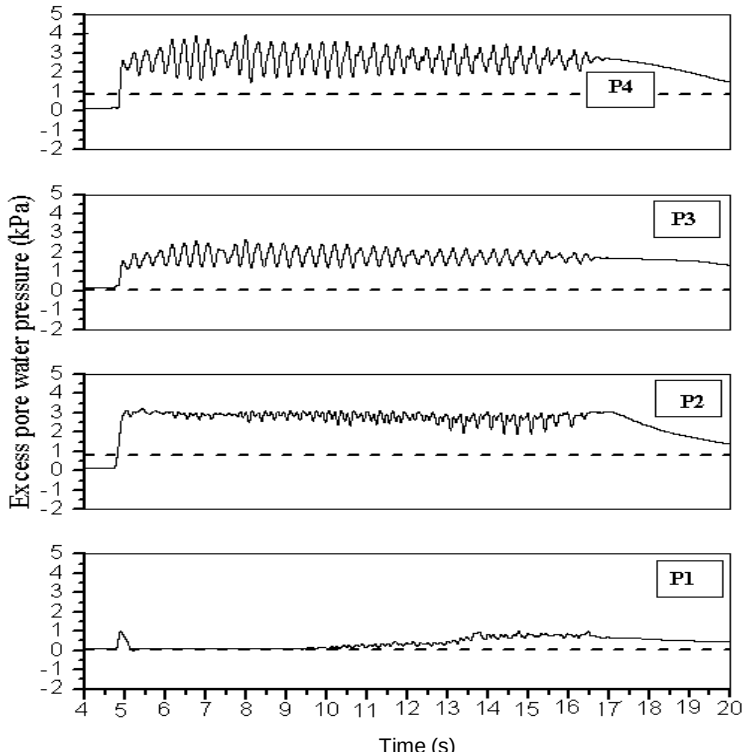

Figure 10. Time histories of excess pore water pressure model 1 (Abdoullah, 2010).

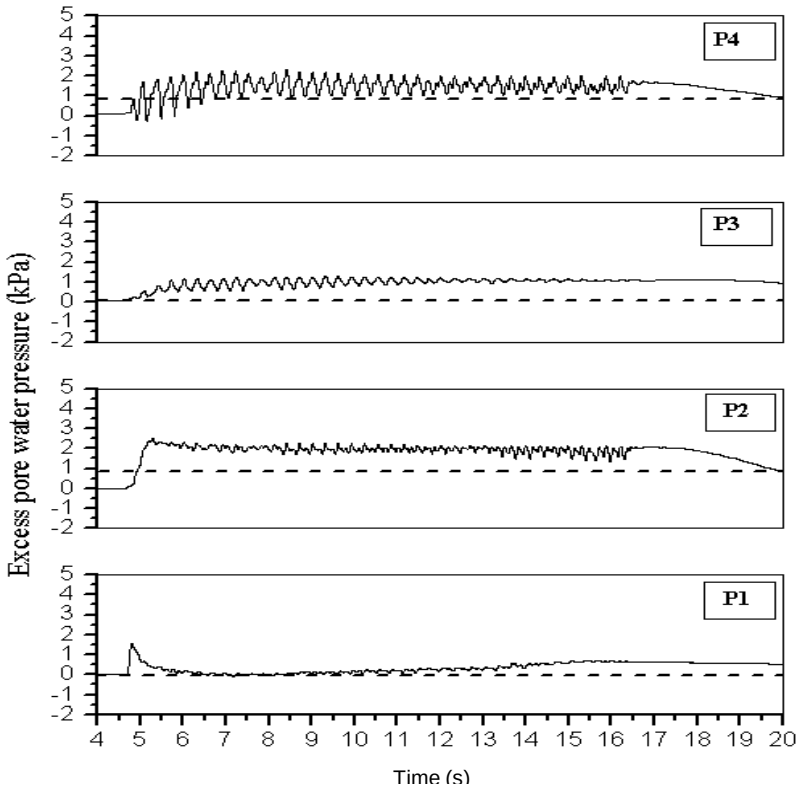

Figure 11. Time histories of excess pore water pressure model 2 (Abdoullah, 2010).

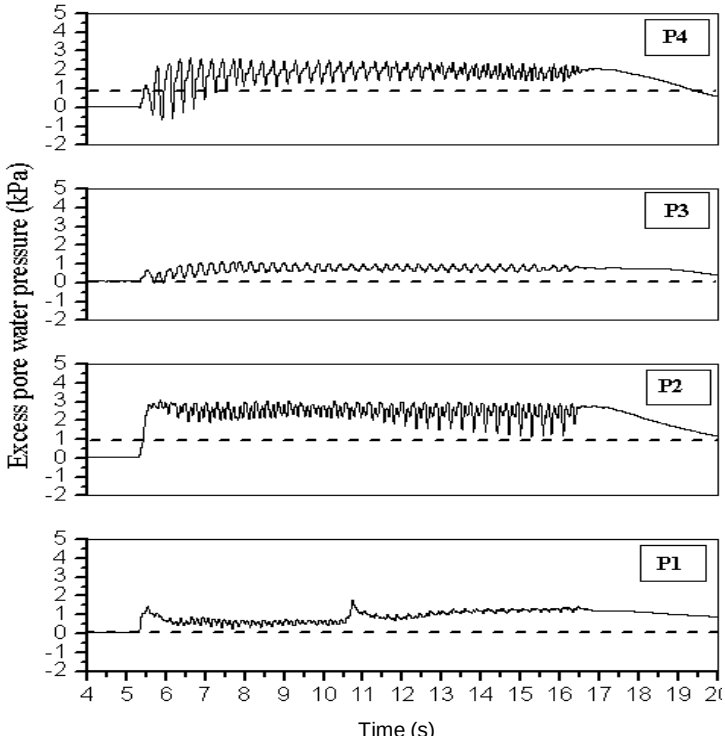

Figure 12. Time histories of excess pore water pressure model 3 (Abdoullah, 2010).

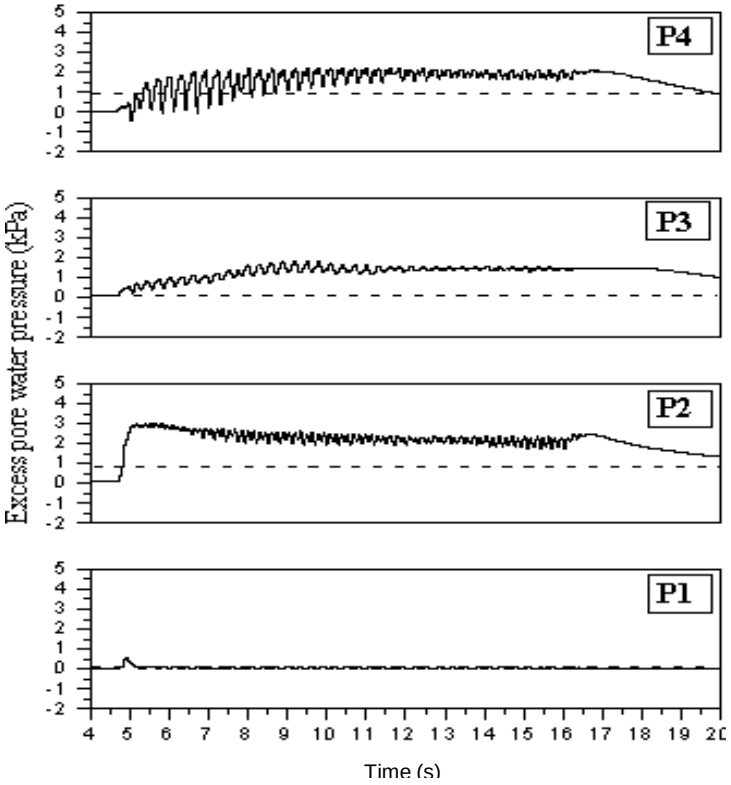

Figure 13. Time histories of excess pore water pressure model 4 (Abdoullah, 2010).

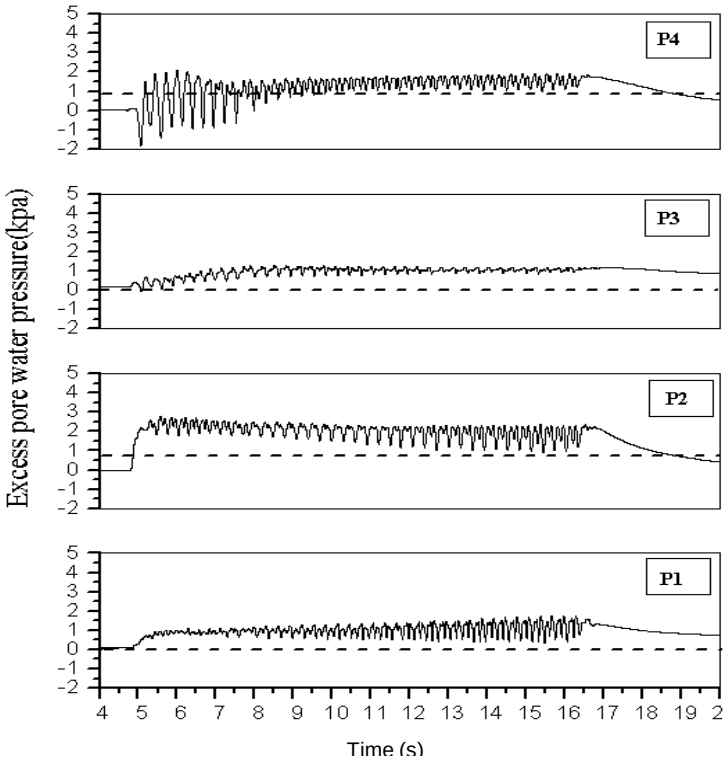

Figure 14. Time histories of excess pore water pressure model 5 (Abdoullah, 2010).

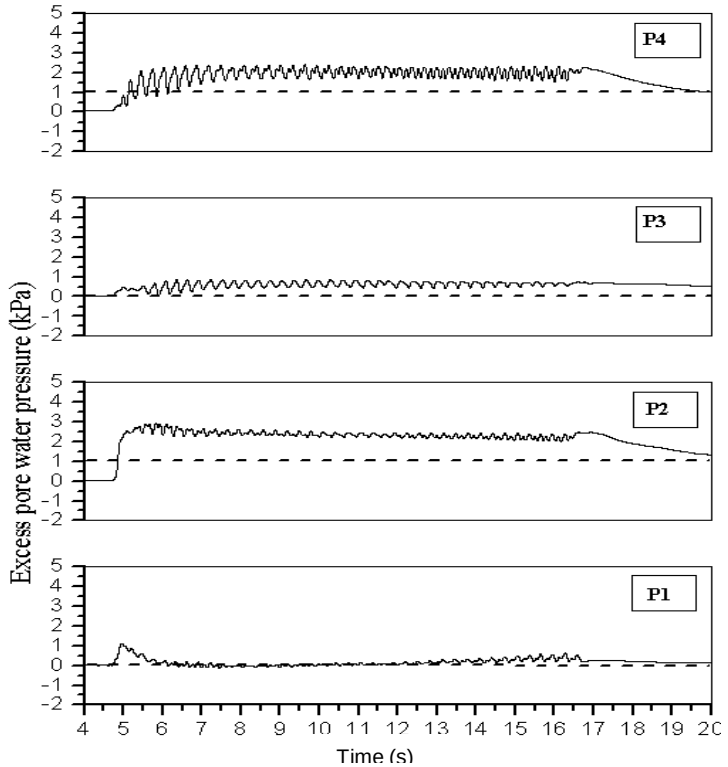

Figure 15. Time histories of excess pore water pressure model 6 (Abdoullah, 2010).

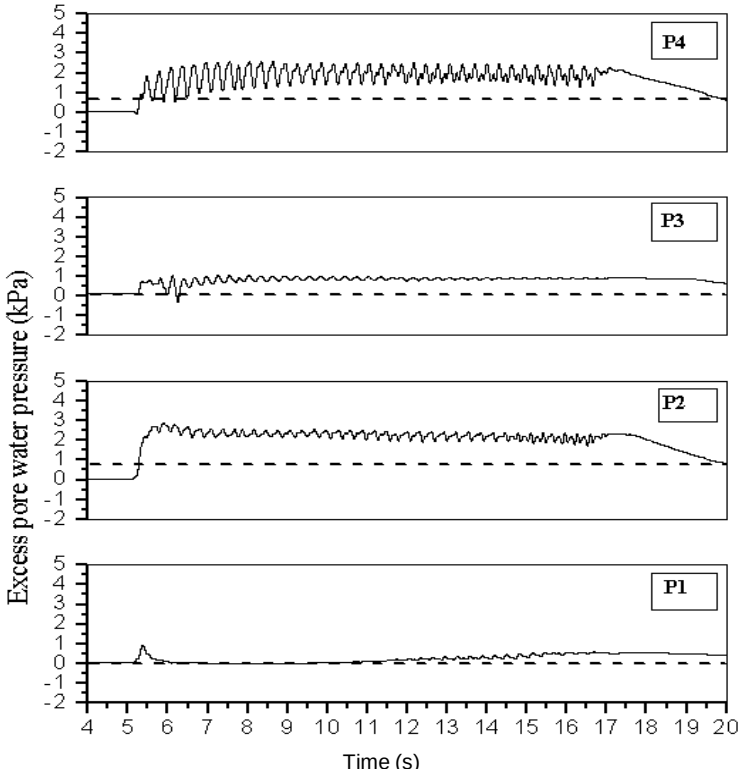

Figure 16. Time histories of excess pore water pressure model 7 (Abdoullah, 2010).

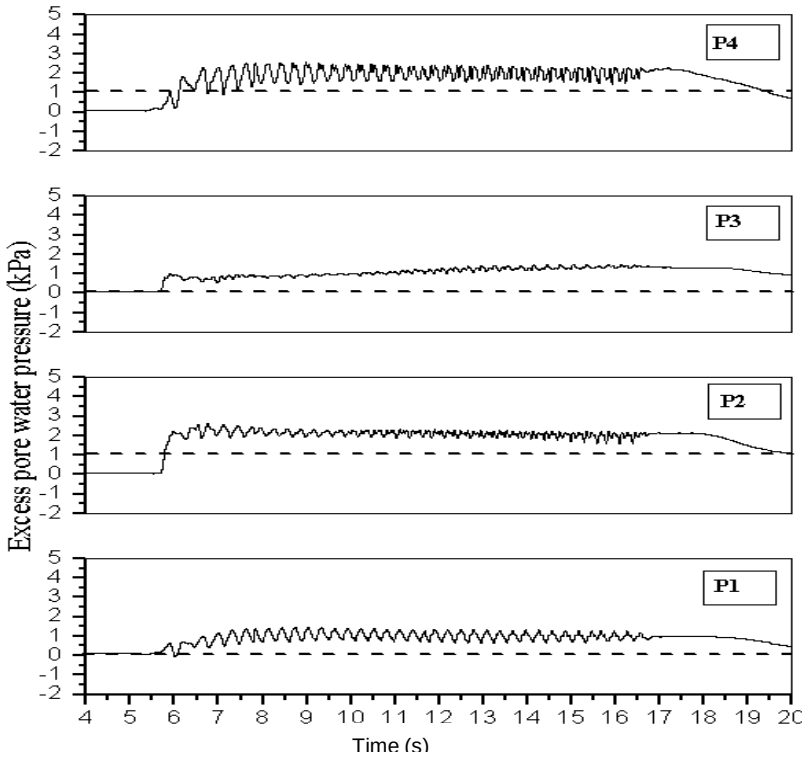

Figure 17. Time histories of excess pore water pressure model 8 (Abdoullah, 2010).

ζ_v = Vertical particle displacement = $\frac{H}{2}\frac{\sinh(ks)}{\sinh(kd)}\cos\theta$ (9)

u = Horizontal particle velocity = $\frac{\pi H}{T}\frac{\cosh(ks)}{\sinh(kd)}\cos\theta$ (10)

w = Vertical particle velocity = $\frac{\pi H}{T}\frac{\sinh(ks)}{\sinh(kd)}\sin\theta$;

$\frac{\partial u}{\partial t}$ = Horizontal particle acceleration = $\frac{2\pi^2 H}{T^2}\frac{\cosh(ks)}{\sinh(kd)}\sin\theta$ (11)

$\frac{\partial w}{\partial t}$ = Vertical particle acceleration = $\frac{2\pi^2 H}{T^2}\frac{\sinh(ks)}{\sinh(kd)}\cos\theta$ (12)

P = Pressure = $-\rho gz + 0.5\,\rho gH\frac{\cosh(ks)}{\cosh(kd)}\cos\theta$ (13)

c_G = Group velocity = $0.5\left[1+\frac{2kd}{\sinh(2kd)}\right]c^2$ (14)

E = Average energy density = $\frac{1}{8}\rho gH^2$ (15)

P_E = Energy flux= $E\,c_G$ (16)

Radiation stress = $S_{xx} = \left[1+\frac{2kd}{\sinh(2kd)}\right]E$ (17)

Radiation stress = $S_{yy} = \left[\frac{2kd}{\sinh(2kd)}\right]E$ (18)

Conclusion

A close agreement between the experimental and numerical results is observed and in the model without dense zone, the maximum liquefaction occurred. The wave theory concept has been used to better explain dynamic liquefaction ability. The result of numerical study is acceptable and it is valid based on previous analytical method. This study indicated that the dense zone could only minimize the differential settlement, and it is not able to convert dynamic pore water pressure to linear force, and as long as dynamic force creates settlement, it is differential settlement. The dynamic pore water pressure act like a wave in vertical direction and if excess higher than limitation causes structure turnover. Then, along with the bending moment the site geological characteristics and some time position of geomembrane also could be a reason for differential settlement or structure overturn.

ACKNOWLEDGEMENTS

The author would like to express thanks to Faculty of Civil Engineering, SJCE, in Mysore for providing laboratory facilities, and express especial appreciate to Professor Syed Shakeeb Ur Rahman Head of Dept of Civil Engineering, SJCE, in Mysore for his timely help and guidance.

REFERENCES

Abdoullah N (2010). Modeling for seismic mitigation of embankment, published by Lambert Academic Publishing, Germany.

Ariman T, Muleski GE (1981). A review of the response of buried pipelines under seismic excitations. Earthquake Eng. Struct. Dyn., 9: 133-151.

Arulmoli K, Muraleetharan KK, Hossain MM, Fruth LS. (1992). VELACS: verification of liquefaction analysis by centrifuge studies; laboratory testing program soil data report. Technical report, the Earth Technology Corporation, Irvine, California.

Ennio Marques Palmeira (2009). Soil–geosynthetic interaction: Modelling and analysis, Geotext. Geomemb., 27: 368-390.

Koseki J, Kawakami S, Nagayama H, Sato T (2000). Change of small strain quasi- elastic deformation properties during undrained cyclic torsional shear and triaxial tests of Toyoura sand. Soils Found., 40(3): 101-10.

Lee JS, Santamarina JC (2007). Seismic monitoring short-duration events: liquefaction in 1g models. Can. Geotech. J., 44:659-72.

Liang J, Sun S (2000). Site effects on seismic behavior of pipelines: a review. ASME J. Pressure Vessel Technol., 122(4): 469-75.

Mostafa A, Sawwaf El (2007). Behavior of strip footing on geogrid-reinforced sand over a soft clay slope, Geotext. Geomemb., 25: 50-60.

Nemat-Nasser S, Tobita Y (1982). Influence of fabric on liquefaction and densification potential of cohesionless sand. Mech. Mater., 1:43-62.

Sivathayalan S. (2000). Fabric, initial state and stress path effects on liquefaction susceptibility of sands. PhD thesis, The University of British Columbia.

Turgut S, Michael I (1981), Mechanics of wave forces on offshore structures, Van Nostrand Reinhold Co, pp. 295-296.

Vaid YP, Chern JC (1985). Cyclic and monotonic undrained response of saturated sands. In: Proceedings of, advances in the art of testing soils under cyclic loading, New York: ASCE, pp. 120-147.

Verdugo R, Ishihara K (1996). Steady state of sandy soils. Soils Found., 36(2): 81-91.